Measurement of Magnetic Fields in Stellar Jets

Patrick Hartigan

Abstract This article reviews magnetic field measurements in jets from young stars, focusing on the physics and application of the three main techniques, Zeeman splitting and polarization, gyrosynchrotron radiation, and the analysis of shocked cooling zones. Estimates of field strengths in stellar jets are rare, and do not refer to the axis of the beam close to the source, where knowledge of the field and its geometry is most critical for constraining launching mechanisms of jets. Nevertheless, the existing measurements demonstrate that magnetic fields in YSO jets are strong enough to be important in the dynamics of the cooling zones behind internal shock waves, even though the ram pressure in the bulk flow dominates the magnetic pressure at large distances from the source. Models of pulsed magnetic flow show that velocity perturbations sweep up the field into dense working surfaces within the jet, increasing the relative importance of magnetic pressure to the dynamics in these regions and reducing its importance in the rarefaction regions that lie between the dense knots.

P. Hartigan (✉)
Physics and Astronomy Department, Rice University, 6100 S. Main, Houston TX 77005, USA
e-mail: hartigan@sparky.rice.edu

K. Tsinganos et al. (eds.), *Protostellar Jets in Context*, Astrophysics and Space Science Proceedings, DOI 10.1007/978-3-642-00576-3_38,

1 Introduction

Many places in the universe that have accretion disks also drive collimated polar jets. Several examples of this process have been discussed at this conference, including jets from young stellar objects (YSOs, [1]), AGNs [16], compact X-ray sources [15], and CVs [23]. YSO jets are a particularly good place to study the phenomenon because the objects are close enough to resolve the widths and collimation properties of jets and study their proper motions. YSO jets radiate emission lines behind shock waves in the flow, and spectra of these lines determine the radial velocities and internal line widths everywhere in these regions (see [20] for a review). In addition, standard nebular diagnostic line ratios provide plasma parameters such as electron densities and temperatures, and it is also possible to learn a great deal about the accretion disk by studying the excess continuum and the emission lines that form as a result of infalling material from the disk onto the star.

How accretion disks drive jets is a major unsolved problem in astrophysics. The available images of YSO jets (e.g. HH 30 [2, 11]) show that jets are already collimated within $\sim$10 AU of the source, much smaller than the size of the disk, ruling out models that rely on the ambient material to focus a spherical wind into a jet [3]. Instead, a structured B field that threads through a rotating disk naturally provides the geometry of a bipolar outflow, and all modern models use magnetic fields in some way to collimate the flow.

Despite the impressive set of observational data described above, one key component of the system is missing, and that is a set of reliable measurements of the magnetic field strength and geometry in the jet. In this paper I will discuss three techniques that various researchers have used to estimate magnetic field strengths in YSO jets (Zeeman, gyrosynchrotron, and shocks) and summarize typical results that emerge from each type of study. It is also possible to infer the existence of aligned grains by polarization measurements of scattered light [4], but inferring field strengths from such data requires models of the dust properties throughout the scattering region which are highly uncertain and beyond the scope of this article.

Ideally we would like to measure field strengths along the axis of jets where the velocity is highest (several hundred km s^{-1}) and where optical emission lines are present that constrain the densities and temperatures in the jet. Unfortunately, none of the available techniques is well-suited for such a measurement. Magnetic fields in YSO jets are too weak to be detected easily with Zeeman splitting in the optical and near-IR, and synchrotron emission is also weak and difficult to interpret. One can use an understanding of radiative shocks to infer field strengths, but this technique has thus far proved effective in only a few cases, and the measurements refer to knots $>$1000 AU from the source, not the collimation region close to the star.

In describing of the physical processes behind each of these techniques I have drawn in part from the excellent textbooks by Rybicki and Lightman [22], Cohen-Tannoudji et al. [5], and Shu [24] for Zeeman splitting and synchrotron radiation. There are several review articles on shock physics, including Draine and

McKee [6] for general description, Ray et al. [20] for recent observations of YSO jets, and Hartigan [8] for physics of magnetic fields and cooling zones in jets, and a previous 'jet-set' contribution for physics of emission line diagnostics [10].

2 Zeeman Splitting

External magnetic fields lift the degeneracy of atomic energy levels by interacting with the dipole moment of a bound electron. This interaction broadens the line by splitting the levels, and the lines have different polarization properties depending on the quantum numbers of the upper and lower levels. This section summarizes how Zeeman splitting works and how it applies to YSO jets.

2.1 Physics: Effect of Magnetic Fields on Energy Levels

Classically, for an electron in a circular orbit, the magnetic dipole moment is $\bar{\mu}$ =**I**A/c, where **I** is the current, and A is the area of the orbit. With **I**=ev/(2πr)$\widehat{z}$ and A= πr^2, we obtain $\bar{\mu}$ =e**L**$_z$/2mc where **L**$_z$ is the angular momentum of the electron perpendicular to its orbit. Substituting **L**$_z$= $\hbar$m$_l$ for the quantum mechanical case we expect typical magnetic splitting to be on the order of μ_BB, where μ_B =e$\hbar$/2mc is the Bohr magneton, 9.26×10^{-21} cgs.

In non-relativistic quantum mechanics with no spin the Hamiltonian for an electron in an atom is

$$\mathbf{H} = \frac{(\mathbf{p} - e\mathbf{A}/c)^2}{2m} + \text{esterms} \tag{1}$$

where esterms are the electrostatic terms between the electron and the nucleus and other electrons. For a uniform external field B$_\circ\hat{z}$, the vector potential is **A**= $-\frac{1}{2}$**r**$\times$ **B**, so that

$$\mathbf{H} = \mathbf{H}_\circ + \mathbf{H}_1 + \mathbf{H}_2 \tag{2}$$

$$\mathbf{H}_\circ = \text{esterms} + \frac{p^2}{2m} \tag{3}$$

$$\mathbf{H}_1 = -\frac{e}{2mc}\mathbf{L} \bullet \mathbf{B} \tag{4}$$

$$\mathbf{H}_2 = \frac{e^2}{8mc^2}(\mathbf{r} \times \mathbf{B})^2 = \frac{e^2}{8mc^2}\left(x^2 + y^2\right) \tag{5}$$

In the above we have used [**p** $\bullet$ (**r**$\times$ **B**) + (**r**$\times$ **B**) $\bullet$ **p**] = [**B** $\bullet$ (**p**$\times$ **r**) + (**p**$\times$ **r**) $\bullet$ **B**] = 2**L** $\bullet$ **B**, with **L** = **r**$\times$ **p**. The terms H$_\circ$, H$_1$ and H$_2$ are, respectively, the unperturbed Hamiltonian, the paramagnetic term, and the diamagnetic term. The diamagnetic term is negligible, so the perturbation becomes

$$\mathbf{H}_1 = -\bar{\mu} \bullet \mathrm{B} = -\frac{\mu_B}{\hbar} \mathrm{L} \bullet \mathrm{B}. \tag{6}$$

Including spin, for each electron i, the magnetic moment is given by

$$\bar{\mu}_i = \frac{\mu_B}{\hbar} \left(\mathbf{l_i} + g_s \mathbf{s_i}\right). \tag{7}$$

In L-S coupling, the total angular momentum operator **J** defines the state. Using

$$\mathbf{L} = \frac{\mathbf{L} \bullet \mathbf{J}}{J^2} \mathbf{J}; \quad \mathbf{S} = \frac{\mathbf{S} \bullet \mathbf{J}}{J^2} \mathbf{J}; \tag{8}$$

and

$$\bar{\mu} = -\frac{\mu_B}{\hbar} \left(\mathbf{L} + 2\mathbf{S}\right) \tag{9}$$

we obtain

$$H_1 = -\frac{\mu_B}{\hbar} g_J \mathbf{J} \bullet \mathbf{B}\,; \quad g_J = \frac{\mathbf{L} \bullet \mathbf{J}}{J^2} + \frac{2\mathbf{S} \bullet \mathbf{J}}{J^2} \tag{10}$$

so that

$$H_1 = -\mu_B B_\circ m_j \left[\frac{3j(j+1) - l(l+1) + s(s+1)}{2j(j+1)}\right] \tag{11}$$

where we have taken the gyromagnetic ratio $g_s = 2.0023 \sim 2$. A typical transition produces a pattern of lines with a characteristic energy splitting $\sim 2\,\mu_B \mathrm{B}$. Converting this energy to a radial velocity Δv we obtain

$$\Delta \mathrm{v} = 5.9 \times 10^{-4} \left(\frac{B}{\mu G}\right) \left(\frac{\lambda}{21\,\mathrm{cm}}\right) \mathrm{km\ s^{-1}} = 2.8 \left(\frac{B}{kG}\right) \left(\frac{\lambda}{1\,\mu\mathrm{m}}\right) \mathrm{km\ s^{-1}} \tag{12}$$

Hence, Zeeman splitting is easiest to detect at longer wavelengths. The strongest fields we expect to see in jets are on the order of a Gauss, so any splitting at optical or infrared wavelengths will be overwhelmed by thermal motions in the gas, which is why no measurements of field strengths are possible from the strong optical and near-IR forbidden lines present along jets.

Figure 1 shows how light emitted by atoms in a magnetic field is polarized. Observer #2 views along the direction of the field and sees the σ components (Δm= $\pm$1) circularly polarized and sees no π (Δm=0) component. In contrast, observer #1 sees linear polarization in the directions indicated. Thus, by subtracting a left-circularly-polarized (LCP) spectrum from its right-handed counterpart (RCP), one can measure the component of the magnetic field along the line of sight. When a magnetic field is present, the difference between the LCP and RCP spectra produces a characteristic signature of a negative residual on one side of the line center and a positive residual on the other side (e.g. [25]). Subtracting the σ and π components does not help observer #1 to measure B because these components have the same average energies and do not reveal the presence of a field until the field is strong enough to clearly separate all three components in the spectrum.

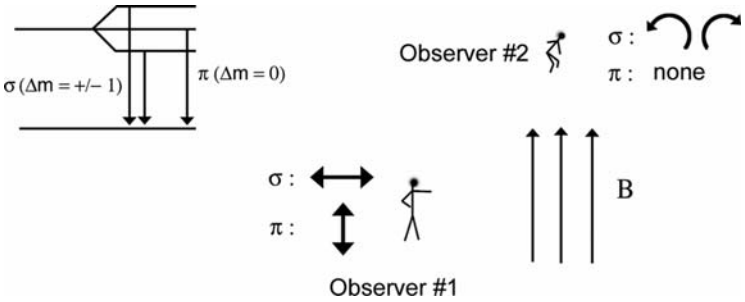

Fig. 1 Polarization of line components in Zeeman splitting

2.2 Line Splitting and Polarization Examples

Most measurements of magnetic fields in star formation regions that make use of Zeeman splitting are at radio wavelengths, where the effect is easiest to measure. Observations of circular polarization at 21 cm in Orion indicate $B_{||} = 174 \pm 20\,\mu G$ [25]. This field produces a very small velocity shift between the LCP and RCP, but is still detectable because 21 cm is a strong line, molecular gas is cold, and radio observations have excellent velocity resolution. Another common application of this technique are observations of masers, where the masing mechanism causes the line emission to peak sharply over a narrow velocity range so it is possible to separate small shifts between the RCP and LCP components. A recent measurement of RCP and LCP in the star formation region W3 by Fish et al. [7] recorded a typical field of 5 mG from the masing regions. While many masers have proper motions and therefore are associated with an outflow, they usually do not define a jet, and are often time-variable and difficult to interpret. A complicating factor is that they usually occur in regions of massive star formation where multiple flows are present and dense filamentary material abounds. Masers are absent in the best examples of YSO jets.

Optical and near-IR measures of fields using Zeeman splitting exist, but because the wavelengths are shorter only strong fields can be detected, and these fields typically arise from the photosphere or in accretion streams that connect the disk to the star. A recent limit of $\sim$30 G for $B_{||}$ in Ae/Be stars using the VLT to measure circular polarization in the Ca II H and K lines illustrates the current limit of the technique for a bright source [14]. A field of 2.5 ± 0.1 kG in the He I emission line of BP Tau was observed by Johns-Krull et al. [12], but this line forms within the accretion columns from the disk onto the star and not within a jet. Observations of absorption line broadening in the near-IR caused by Zeeman splitting exist for young stars [13], and are typically 2.5 kG. These fields come from starspots on the stellar photosphere. The observations are based on line widths rather than on polarizations, so have the advantage of being independent of the field geometry, but are limited to strong fields because absorption lines are broadened by rotation.

3 Synchrotron and Cyclotron Emission

When electrons spiral around a magnetic field lines the electrons are accelerated by the Lorentz force and emit radiation. Measuring the flux, spectral energy distribution, and polarization properties of the emitted light constrains the strength and geometry of the magnetic field. The technique has been limited to date by the relative rarity of this emission from stellar jets, but could hold more promise in the future. This section summarizes the cyclotron, gyrosynchrotron, and synchrotron emission process as they apply to YSO jets.

3.1 Physics: Continuum Emission from Particles in a Magnetic Field

An accelerated charge radiates linearly polarized light in a direction perpendicular to the acceleration. As described by Rybicki and Lightman [22], there is a straighftorward way to see why this must occur. A charged particle at rest at the origin will have electric field lines that point radially away from the origin. If the particle receives a sudden impulse in the x-direction so that it moves at a constant velocity, the information about the impulse travels outward from the origin at the speed of light. Within this light sphere the retarded potentials show that the electric field points to the current position of the particle. This remarkable result implies that except along the x-axis, where the field is always in the $\pm\widehat{x}$ direction, the electric field must bend suddenly at the light sphere. As a result, the electric field has a perpendicular component at the light sphere proportional to 1/r, and therefore must radiate because there is a non-zero Poynting flux at large distances. An observer at infinity sees linearly polarized light along the projected direction of the acceleration vector.

An electron moving in an external magnetic field B feels a Lorentz force perpendicular to its direction of motion that causes it to spiral around the field line with an angular frequency $\omega_B = \mathrm{eB}/\gamma\mathrm{mc}$. For the non-relativistic case (cyclotron, $\gamma \sim 1$), an external observer sees a sinusoidal electric field in the emitted radiation, and the power spectrum of this is a single emission 'line' at the cyclotron frequency ω_B. However, as γ increases, the electron will progressively beam radiation in the forward direction, so the observed electric field in still periodic, but no longer sinusoidal. The Fourier transform of such a function consists of the harmonics of the gyration frequency, $\omega = \mathrm{n}\omega_B$, where n is an integer. The peak of the harmonics occurs at $\omega_C \sim \gamma^3\omega_B \sin\alpha$, where α is the pitch angle of the particle's motion in the field [22]. The resulting emission is highly linearly polarized perpendicular to the field direction. For a more realistic case of a power law energy distribution of electrons ($\mathrm{n(E)}\sim\mathrm{E}^{-p}$), the spectrum is also a power law with index $\mathrm{s} = (\mathrm{p}-1)/2$, and the total emitted power is proportional to B^k with $\mathrm{k} = (\mathrm{p}+1)/2$.

When $\gamma \gg 1$ (synchrotron), the emission is strongly beamed into a narrow cone along its direction of motion. Hence, an observer sees almost all the radiation as

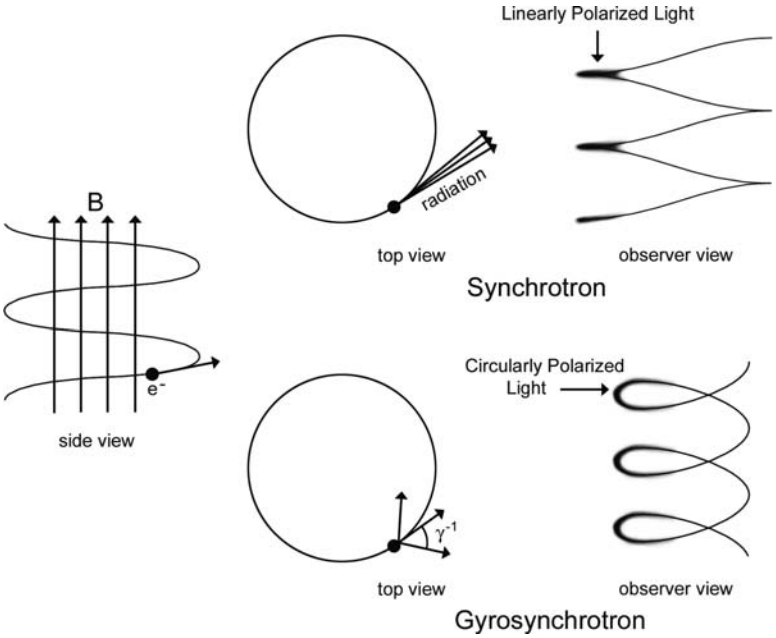

Fig. 2 Geometry of synchrotron and gyrosynchrotron emission. An electron spirals around a uniform magnetic field as shown in the side view. The radiation is emitted in the forward and reverse direction of the electron's motion, perpendicular to the direction of acceleration. Top: For synchrotron emission the electron is highly relativistic, so most of the emission is beamed in a narrow cone aligned with the direction of motion. Hence, the electron's velocity vector must point almost directly toward the observer at some point in its gyration about the field, so the observer sees the path of the electron as indicated at right, and the radiation is mainly linearly polarized. Bottom: For gyrosynchrotron $\gamma \sim 1$, so the opening angle of the emission cone is much wider. Thus, an observer typically sees radiation along a curved path in the sky as shown in the bottom right, implying circular polarization

arising from a small angular section of the orbital spiral where the motion of the electron points almost directly at the observer (Fig. 2, top). The apparent motion of the electron over this section as seen by the observer is linear, so the emitted light is linearly polarized. Synchrotron sources have little circular polarization because LCP and RCP radiation occur in equal amounts from electrons whose cones of emission lie just a bit above and below our line of sight, respectively.

However, in the intermediate case of gyrosynchrotron emission ($1 < \gamma < 3$) the emission is only moderately beamed, so the cone of emission is wide enough to allow an observer to see the circular motion of the electron during the emission process, and the emitted light retains a circularly polarized component unless the viewing angle happens to be exactly perpendicular to the field lines (Fig. 2, bottom). The amount of this circular polarization depends on the power law index, the pitch angle, and γ, but with reasonable bounds of these parameters one can at least obtain an order of magnitude estimate of the magnetic field strength.

3.2 The Case of T Tauri-S

Observations of circular polarization in YSO jets are rare. The best example is that of Ray et al. [19], who detected LCP and RCP emission in 6 cm observations of the companion to T Tauri. The polarized emission was offset on either side of the star, suggestive of an ordered field structure away from the photosphere. The field strength was on the order of a few Gauss, assuming a typical range for the unknown pitch angles, γ, and power law index.

While intriguing, this measurement is difficult to interpret because the spatial resolution of the observations is similar to the offset of the emission from the star, so a jet geometry is not necessarily implied by the observations. If the emission does arise in a jet, it probably comes from a strong shock close to the star, and then the average field in the jet will be much lower.

4 Magnetic Pressure in Cooling Zones of Shocks

This section outlines how one can combine the large number of emission lines present behind shocks in jets with detailed kinematic information about velocities to facilitate measurements of magnetic fields.

4.1 Physics: Magnetic Pressure in Postshock Cooling Zones

Estimating field strengths within radiative shocks is in principle a straightforward concept. If we know the shock velocity and the preshock density, then conserving mass, momentum and energy across the shock implies that the density increases by a factor of four in a strong atomic shock [6]. Since the magnetic field is tied to the fluid, the component of the field that lies parallel to the shock front (perpendicular to the normal) must also increase by a factor of four. As the gas cools it compresses, and the magnetic field rises in proportion to the density.

Because the magnetic pressure $P_m \sim B^2 \sim \rho^2$ where B is the field strength and ρ the density, the ratio $P_m/P_{gas} \sim \rho$. This ratio increases in the postshock zone until the magnetic pressure dominates in the dense cooling zone, even if the initial field was dynamically unimportant (i.e., $B^2/8\pi \ll \rho v^2$. Hence, it is possible to infer a field strength by comparing the observed density in the cooling zone with that expected for a nonmagnetic shock [8].

4.2 Application of Cooling Zone Method to Stellar Jets

While simple in principle, applying the above method requires the shock to have a relatively simple geometry, and have a well-defined shock velocity and preshock

density. Shocks in YSO jets often exhibit complex morphologies, but examples also exist of well-defined bow shocks. Estimating a shock velocity is possible by combining the observed line ratios with the shape of the bow shock. It is easiest to do this if the bow shock is strong enough to emit [O III] lines, which only occur when the shock velocity exceeds $\sim 90\,\mathrm{km\,s^{-1}}$. Essentially the point where the shock velocity drops below this value is marked by the edge of the [O III] emission along the bow shock, and the shape of the bow then gives the shock velocity. The preshock density is then measured from the total line fluxes, which must be dereddened. Finally, one can measure the electron density from emission line ratios of [S II] (see e.g. [10]), which implies a total density from the ionization fraction estimated from other emission lines. While uncertainties exist in all these measurements, the difference between the observed density in the cooling zone and that expected for a nonmagnetic shock is typically an order of magnitude, so the presence of even a weak field is easy to detect.

Morse et al. [17, 18] applied the above method to two YSO jets and found $B \sim 15\,\mu\,G$ for the preshock gas in front of major bow shocks in the flows, and about a factor of 10 higher in the postshock gas. These bow shocks are located $\sim 5 \times 10^4$ AU from the source, so to infer anything about the field strength close to the source we need to understand how the field strength varies with distance in a typical YSO jet. A recent study that focuses on this issue is described in the next section.

5 Implications for a Velocity-Variable Magnetic Flow

The standard picture of a magnetized jet is that the field is anchored in the accretion disk and becomes increasingly toroidal as the jet becomes collimated. However, if the field is too strong, then it will inhibit the formation of shocks. We observe shock waves at 10^5 AU when velocity pulses are only $\sim 30\,\mathrm{km\,s^{-1}}$, so the fields there must be less than about a mG, consistent with those estimated from the cooling zone method described above. Closer to the sources, the ~ 1 G fields found from the circular polarization measurements imply a stronger field.

Are the weak fields observed at large distances (10^4–10^5 AU) consistent with stronger fields inferred within the acceleration regions (~ 10 AU) of YSO jets? Jets appear to expand at roughly a constant opening angle, so the average density declines with distance from the source approximately as r^{-2}. For a toroidally dominated disk wind, $B \sim r^{-1} \sim n^{0.5}$, so the magnetic signal speed, which is governed by longitudinal magnetosonic waves, should be roughly constant in such a flow. However, within a shock wave $B \sim n$, so we might expect $B \sim r^{-2}$ in these regions. This steeper dependence of B on r would help to reconcile strong fields close to the star with weaker fields at large distances.

Recent models of magnetized pulsed outflows show that they behave in a manner intermediate between the disk wind and shock limits described above [9]. Essentially velocity pulses in the jet sweep up the field into a few dense knots, and create rarefactions between the knots. Within rarefactions the magnetic signal speed drops

markedly, which makes shock waves possible in the flow. The models which best reproduce the observed shock velocities are ones where the terminal magnetosonic Mach number of the flow is ~ 5. Lower terminal magnetosonic Mach numbers are unable to produce both the high velocities of the jets and the low shock velocities present in the velocity perturbations (small amplitude perturbations become magnetic waves rather than MHD shocks).

6 Summary

Despite their probable importance in YSO jets, magnetic fields have proved elusive to measure in these objects. Nonetheless, field estimates do exist, and the available measurements appear to be generally consistent with the notion of a jet driven magnetically from the source, with velocity pulses playing an important role in sweeping the field into a few dense regions, and areas of much lower field prevailing between the knots. Dynamically the field is strong enough in the dense knots to dominate the pressure, but must be significantly lower than the overall ram pressure of the flow in order to allow the weak shocks observed, which have shock velocities only $\sim 10\%$ of the flow speed.

Probably the most exciting future prospect for measuring field strengths in YSO jets is Zeeman splitting of molecular lines with ALMA (see the article by Richer in this volume [21]). While this technique will only be applicable to the youngest jets such as HH 212 which have strong molecular emission along the axis of the flow, any additional quantitative measurements of field strengths in these jets will go a long way to clarifying how YSO jets become collimated and how they are driven by their accretion disks.

Acknowledgements This research was supported by NASA Origins of Solar System Grant NNG05GH97G to PMH.

References

1. Bally, J. 2009, in *Protostellar Jets in Context*, K. Tsinganos, T. Ray & M. Stute eds., (New York:Springer)
2. Burrows, C. et al. 1996, ApJ, 473, 437
3. Canto, J. 1980, A&A, 86, 982
4. Chrysostomou, A., Lucas, P., & Hough, J. 2007, Nature, 450, 71
5. Cohen-Tannoudji, C., Diu, B., & Laloë, F. 1977, *Quantum Mechanics*, (New York:John Wiley and Sons)
6. Draine, B., & McKee, C. 1993, ARA&A, 31, 373
7. Fish, V., Brisken, W., & Sjouwerman, L. 2006, ApJ, 647, 418
8. Hartigan, P. 2003, Ap&SS, 287, 111
9. Hartigan, P., Frank, A., Varniere, P., & Blackman, E. 2007, ApJ, 661, 910
10. Hartigan, P. 2008, *Jets From Young Stars II*, Lecture Notes in Physics, 742, 15
11. Hartigan, P., & Morse, J. 2007, ApJ, 660, 426

12. Johns-Krull, C., Valenti, J., Hatzes, A., & Kanaan, A. 1999, ApJ, 510, L41
13. Johns-Krull, C., Valenti, J., & Saar, S. 1999, ApJ, 617, 1204
14. Hubrig, S., Yudin, R., Schöller, M., & Pogodin, M. 2006, A&A, 446, 1089
15. Livio, M. 2009, in *Protostellar Jets in Context*, K. Tsinganos, T. Ray & M. Stute eds., (New York:Springer)
16. Massaglia, S. 2009, in *Protostellar Jets in Context*, K. Tsinganos, T. Ray & M. Stute eds., (New York:Springer)
17. Morse, J., Hartigan, P., Cecil, G., Raymond, J., & Heathcote, S. 1992, ApJ, 399, 231
18. Morse, J., Heathcote, S., Cecil, G., Hartigan, P., & Raymond, J. 1993, ApJ, 410, 764
19. Ray, T., Muxlow, T. W. B., Axon, D. J., Brown, A., Corcoran, D., Dyson, J., & Mundt, R. 1997, Nature, 385, 415
20. Ray, T., Dougados, C., Bacciotti, F., Eislöffel, J., & Chrysostomou, A. 2006, in *Protostars and Planets V*, B. Reipurth, D. Jewitt, & K. Keil eds., (Tucson:University of Arizona Press).
21. Richer, J. 2009, in *Protostellar Jets in Context*, K. Tsinganos, T. Ray & M. Stute eds., (New York:Springer)
22. Rybicki, G., & Lightman, A. 1979, *Radiative Processes in Astrophysics*, (New York: John Wiley and Sons)
23. Sokoloski, J. 2009, in *Protostellar Jets in Context*, K. Tsinganos, T. Ray & M. Stute eds., (New York:Springer)
24. Shu, F. 1991, *The Physics of Astrophysics Volume 1: Radiation*, (Mill Valley CA:University Science Books).
25. Troland, T., Heiles, C., & Goss, W. 1989, ApJ, 337, 342